Chemical Tuning of Exciton versus Charge-Transfer Excited States in Conformationally Restricted Arylene Cages

Taylor N. Lewis,[§] Claire Tonnelé,[‡] William G. Shuler,[†] Zachary A. Kasun,[†] Hiroki Sato,[†] Adam Berges,[§] Jacob R. Rodriguez,[⸸] Michael J. Krische,*[†] David Casanova*[‡ǂ] and Christopher J. Bardeen*[⸸§]

[§]University of California, Riverside, Department of Chemistry, Riverside, CA 92521, USA

[‡]Donostia International Physics Center (DIPC) 20018, Donostia, Euskadi, Spain

[†]University of Texas at Austin, Department of Chemistry, Austin, TX 78712, USA

[⸸]University of California, Riverside, Department of Materials Science and Engineering, Riverside, CA 92521, USA

[ǂ]IKERBASQUE – Basque Foundation for Science, 48009, Bilbao, Euskadi, Spain

Supporting Information Placeholder

ABSTRACT: Covalent assemblies of conjugated organic chromophores provide the opportunity to engineer new excited states with novel properties. In this work, a newly developed triple-stranded cage architecture, in which meta-substituted aromatic caps serve as covalent linking groups that attach to both top and bottom of the conjugated molecule walls, is used to tune the properties of thiophene oligomer assemblies. Benzene-capped and triazine-capped 5,5'-(2,2-bithiophene)-containing arylene cages are synthesized and characterized using steady-state and time-resolved spectroscopic methods. The conformational freedom and electronic states are analyzed using time-dependent density functional theory. The benzene cap acts as a passive spacer whose electronic states do not mix with those of the chromophore walls. The excited state properties are dominated by through-space interactions between the chromophore subunits, generating a neutral Frenkel H-type exciton state. This excitonic state undergoes intersystem crossing on a 200 ps timescale while the fluorescence output is suppressed by a factor of 2 due to a decreased radiative rate. Switching to a triazine cap enables electron transfer from the chromophore-linker after the initial excitation to the exciton state, leading to the formation of a charge-transfer state within 10 picoseconds. This state can avoid intersystem crossing and exhibits red-shifted fluorescence with enhanced quantum yield. The ability to interchange structural modules with different electronic properties while retaining the overall cage morphology provides a new approach for tuning the properties of discrete chromophore assemblies.

INTRODUCTION

The properties of organic electronic materials are determined by interactions between their conjugated subunits, for example molecules in a crystal or polymer repeat units in an amorphous film.[1] One major challenge in this field lies in understanding and controlling these interactions, which can give rise to new emergent properties of the assembly. For example, when multiple organic chromophores interact, new electronic states that support delocalized excitons or separated electron-hole pairs can arise due to dipole-dipole and electron transfer interactions. In bulk solid-state samples, disorder and the large number of interacting molecules make it challenging to achieve a first-principles understanding of these new states. The complexity of the solid-state has motivated the study of smaller systems that can be purified and studied in isolation, for example in dilute solution. Examples of such conjugated assemblies include donor-bridge-acceptor molecules and covalent chromophore assemblies like bichromophores and dendrimers.[2-13] In these supermolecules, covalent linker groups define both the number and connectivity of the interacting conjugated subunits.

The ability to synthesize discrete multiunit assemblies of conjugated molecules unlocks the ability to study complicated multi-body phenomena like singlet fission[14-21] with a high level of experimental and computational sophistication. However, conformational flexibility in these covalent assemblies can lead to multiple configurations that have different sub-unit interactions and thus different electronic states and dynamics. In many cases, the conformational freedom of these covalent assemblies complicates their interpretation as structurally well-defined model systems.[22-26] A second problem concerns the role played by the covalent linker group in the electronic structure and dynamics. Although it is most convenient to assume that the linker is inert, there now exists a large body of work showing that it can play an important role in facilitating charge and energy transfer.[27-36] Given these complications, it is desirable to design a covalent multi-chromophore architecture that 1) provides additional limits on the conformational freedom of the constituent chromophores; and 2) allows a modular approach to vary the chemical structure of the linker group and systematically explore its role in determining the electronic properties of the assembly.

In this work, we utilize a novel cage architecture for creating assemblies of conjugated organic chromophores. Meta-substituted aromatic caps serve as the covalent linking groups that attach to both top and bottom of the conjugated sub-unit. This strategy enables improved control of both molecular spacing and orientation because it provides two points of attachment for each conjugated subunit, bringing the assembly closer to crystalline order. Furthermore, the capping group acts as a constant structural element while providing chemical tunability that can be used to actively modify the electronic structure of the assembly. To illustrate this strategy, Figure 1 presents two possible implementations of the cage structures with capping units that

can support either neutral exciton or CT states.

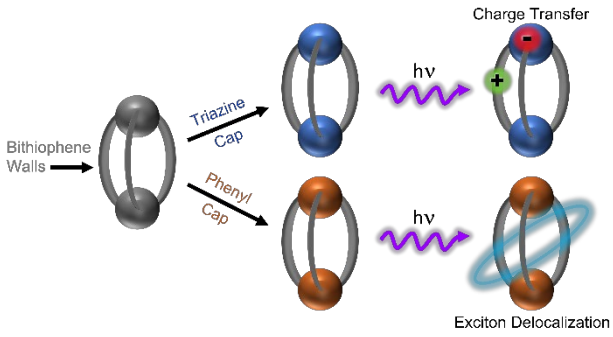

Figure 1. Schematic of capped bithiophene cage. Dependent on the capping unit used to lock the bithiophenes into the cage conformation, it can undergo charge transfer or exciton delocalization.

To demonstrate the capabilities of the architecture shown in Figure 1, in this paper we study the properties of a bithiophene trimer built as a cage with two different aromatic capping units. The use of a simple phenyl cap leads to the generation of a Frenkel H-type exciton excited state with a reduced radiative rate and lowered fluorescence yield. This is an example of a passive capping group whose electronic states do not mix with those of the chromophore walls. The excited state properties are dominated by through-space interactions between the chromophore subunits themselves. On the other hand, switching to a triazine cap provides the opportunity for chromophore-linker electron transfer and leads to the formation of new CT states with enhanced fluorescence. The ability to create different nanoscale heterostructures while retaining the overall morphology provides an unprecedented opportunity to tune the properties of these discrete assemblies. This architecture is in principle scalable and may provide a path to systematically bridge the gap between molecular properties and solid-state material performance.

RESULTS

Synthesis of Arylene Cages 4a and 4b and Model Compounds 6a and 6b

Using a ruthenium-catalyzed diol-diene [4+2] cycloaddition[37], a protocol for benzannulation was developed in the laboratory one of the present authors.[38] This method opened novel synthetic routes to diverse polycyclic aromatic hydrocarbons: acenes and fluoranthenes[38], oligo(*o,p*-phenylenes) and, therefrom, nanographenes[39], diindenoperylenes (periflanthenes)[40], rubicenes[41], and a novel class of triple helical phenylene cages[42], including an all-aryl caged *fac*-Ir(ppy)$_3$ analog.[43] The relatively rigid topology of the arylene cages and the roughly orthogonal orientation of their walls vs caps inspired the design of the cages **4a** (Z = CH) and **4b** (Z = N), which have 5,5-(2,2-bithiophene) walls terminated by 1,3,5-benzene or s-triazine caps, respectively. The choice of thiophene walls was inspired by the fact that thiophene oligomers and polymers comprise an important family of organic semiconductors that have seen wide application in devices like photovoltaic cells and transistors. There has been extensive previous work on covalent thiophene assemblies, like dendrimers, that support energy migration[44, 45] and charge separation[46-48] and have even been used in bulk heterojunction photovoltaics.[49, 50] But so far there has been no effort to create a single structural motif that can be engineered to serve either purpose.

The procedure for synthesizing the thiophene cage compounds is summarized in Scheme 1. The all-benzene cages were prepared via dimerization of a *tris*-bromide[42, 43], requiring use of the ruthenium-catalyzed diol-diene benzannulation protocol due to its compatibility with aryl bromide functional groups. As thiophenes undergo efficient bromination at the 2-position[51], the preparation of the benzene-capped 2,2-bithiophene cage **4a** was more directly achieved via threefold Suzuki coupling of 1,3,5-tribromobenzene 1a[52] and 2-thienylboronic acid 2 followed by threefold *N*-bromosuccinimide (NBS)-mediated bromination to form the *tris*-bromide 3a. The latter reaction was conducted in $CDCl_3$ to enable monitoring of the reaction by ^{1}H NMR, as the *tris*-bromide 3a is not separable from the corresponding mono- and dibrominated compounds. Threefold reductive dimerization of *tris*-bromide 3a to form the benzene-capped cage **4a** via the Lipshutz cuprate, $[Ar_2Cu(CN)Li_2]$[53] (as described by Iyoda)[54-58], and related methods involving direct threefold lithiation of the thiophene C-H bond adjacent to sulfur followed by $CuCl_2$ or $FeCl_3$-mediated dimerization[59, 60], were complicated by the formation of inseparable impurities. In contrast, threefold nickel(0)-mediated reductive dimerization [61-64] delivered the benzene-capped cage **4a** in 34% yield. In similar manner, threefold Suzuki coupling of cyanuric chloride 1b[52, 65, 66] and 2-thienylboronic acid 2 followed by threefold bromination mediated by *N*-bromosuccinimide (NBS) delivered *tris*-bromide 3b, which upon nickel(0)-mediated threefold reductive

Scheme 1. Synthesis of triazine-capped and benzene-capped 5,5'-(2,2-bithiophene)-containing arylene cages 4a and 4b.

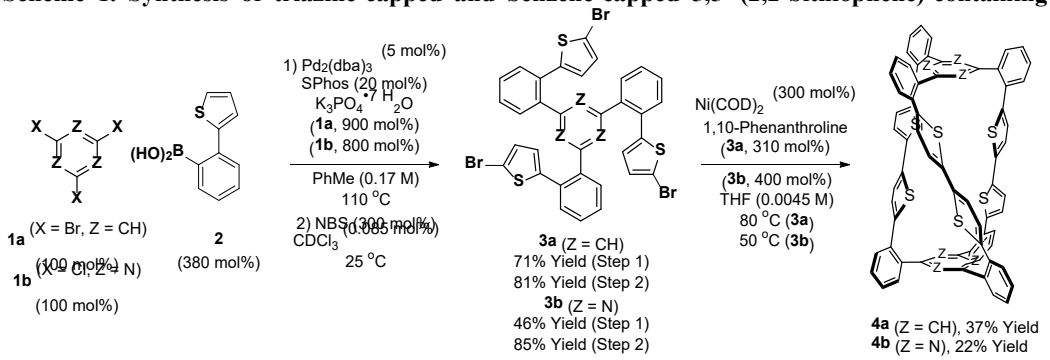

Yields of material isolated by silica gel chromatography. See Supporting Information for further experimental details.

dimerization delivered the triazine-capped donor-accepter cage **4b** in 22% yield (Scheme 1). Cages **4a** and **4b** could be crystallized via vapor diffusion of hexanes into dichloromethane and pentane into chloroform, respectively, allowing their structures to be corroborated by single crystal X-ray diffraction analysis (Figure 2). The cage structures are chiral, but at room temperature they appear to interconvert too rapidly to be resolved as separate species in NMR experiments or by chromatography.[43] Finally, 2,2'-bithiophene model compounds **6a** and **6b**, which are terminated by phenyl and diphenyltriazine moieties, respectively, were prepared via direct 2-lithiation of the mono-thiophene precursors 5a and 5b followed by $FeCl_3$-mediated dimerization (Scheme 2).[60]

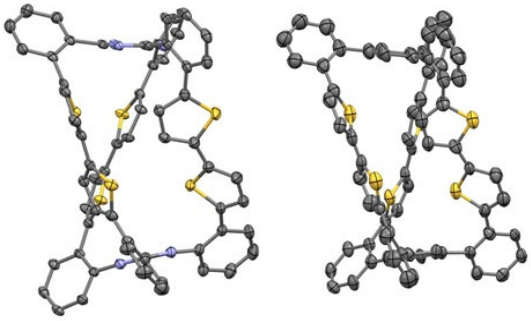

Figure 2. Single-crystal X-ray diffraction data of arylene cages **4b** (Left) and **4a** (Right). Displacement ellipsoids are scaled to the 50% probability level. Hydrogen atoms and solvent have been omitted for clarity.

Scheme 2. Synthesis of triazine-terminated and benzene- terminated model compounds 6a and 6b corresponding to dithiophene-containing arylene cages 4a and 4b.

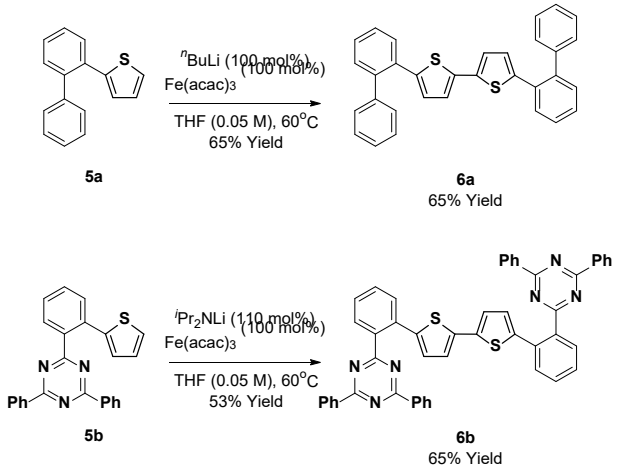

Photophysical Properties of Arylene Cages 4a and 4b and Related Computational Studies

A. Evaluation of Conformational Disorder

It was posited that the geometric and conformational constraints of the present triple helical cage architectures would restrict the composite chromophores in a roughly orthogonal arrangement. Computational geometry optimization was used to compare the geometries for the studied monomers and cages. We found several different minima on their respective ground state potential energy surfaces. Due to the absence of the cage structure, 8 different conformations of monomer **6a** are accessible at room temperature, as a low rotational barrier is associated with the biaryl linkage between benzene and thiophene moieties (Supporting Information, Figure SI-4 and Table SI-13). The steric hindrance associated with the larger triazine moiety reduces the configuration space energetically accessible in monomer **6b**, for which two quasi-isoenergetic conformers (ΔE = 0.7 kcal/mol) are found (Supporting Information, Figure SI-6 and Table SI-14). The cage architecture provides different steric constraints, and two quasi-isoenergetic (ΔE = 0.8 kcal/mol) conformations were found for compounds **4a** (Supporting Information, Figure SI-7) and **4b** (Supporting Information, Figure SI-7 and Table SI-15). To put these results in perspective, if we considered three chromophores, each able to freely adopt two conformations, we would naively expect to have 2^3=8 local energy minima for the assemblies. In our computational search, we were only able to find two low-energy minima for **4a** and **4b** (within a given enantiomer of the triple helix), a remarkable reduction in the available phase space for these chromophores.

Figure 3. Histogram of the distribution of the changes in excitation

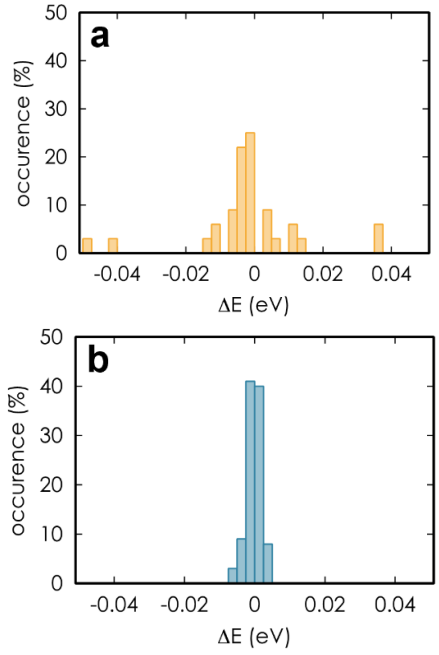

energy to the S1 state of compound **6a** (a) and cage **4a** (b) upon thermal activation of the low-frequency modes.

The cage structure has the most pronounced effect on the conformational dynamics and electronic heterogeneity of the chromophores. Compounds **6a** and **6b** are structurally flexible with numerous quite flat vibrational modes involving different rotational motions and the relative torsion of conjugated rings. These molecular motions are notably restricted by the cage structure in **4a** and **4b**. The suppression of the low-frequency modes in **4a** and **4b** with respect to the monomeric compounds becomes evident when exploring the variation of vertical excitation energies at the Franck-Condon geometry triggered by

molecular vibrations (Figure 3). The results clearly show that thermal activation of the low-frequency modes induces a much larger variation of the S_0-S_1 gap in **6a** than in cage **4a**. Again, theory confirms the general trend of reduced conformational freedom and narrower energy distributions for the cage structures, despite the presence of three chromophores instead of one.

B. Inert Phenyl Linkers and Frenkel Exciton Formation in Compounds 4a and 6a

Due to the substantial vibronic coupling in the thiophenes, the reduced conformational freedom did not lead to an observable narrowing of the absorption spectrum, as shown in Figure 4a. Comparing the cage compound **4a** to the monomer **6a**, both spectra are featureless Gaussian-type peaks with a full-width-half-maximum of about 70 nm. The cage exhibits a slight blueshift of the main peak, along with the appearance of a red-shifted shoulder past 400 nm. This change in absorption lineshape is a classic sign of H-type aggregation. In the standard Kasha model, side-by-side transition dipole moments (TDMs) interact to split the original monomer excited state into a strongly allowed exciton state at higher energy and a weaker state at lower energy.[67] This side-by-side geometry is created by the bithiophene cage walls. The absorption and fluorescence spectra of **4a** and **6a** are insensitive to solvent polarity (Supporting Information, Figure SI-12), consistent with little or no CT character.

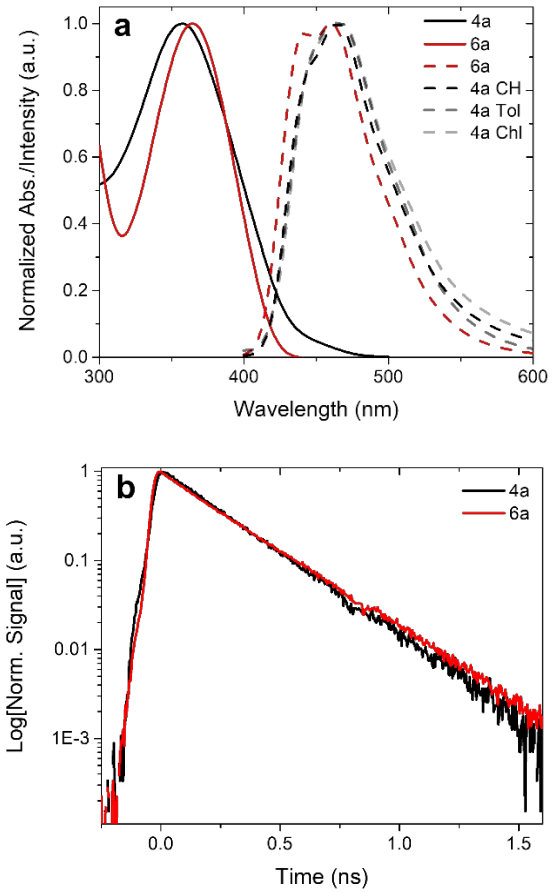

Figure 4. (a) UV-vis absorption (solid) and emission (dashed) spectra of phenyl-capped bithiophene cage (**4a**, black) and phenyl-capped monomer (**6a**, red). The emission of **4a** is shown in three solvents, cyclohexane (CH), toluene (Tol), and chloroform (Chl), to show no shift in the emission as solvent polarity increases. For the emission spectra, a 350 nm excitation wavelength was used. (b) Fluorescence decays of cage **4a** (black) and monomer **6a** (red) are almost identical.

Additional experimental evidence for neutral, H-type excitons is provided by examination of the fluorescence spectrum. The 0-0 vibronic peak, which is clearly visible in **6a**'s fluorescence spectrum as a peak at 430 nm, is diminished in the spectrum of **4a**, where it now appears as a shoulder. By fitting each of the emission spectra to a set of three Gaussians with an equal spacing of 1350 cm^{-1} (Supporting Information, Figure SI-14), we find that the amplitude **4a**'s 0-0 peak decreases by ~20% relative to that of **6a**. This loss of intensity in the 0-0 peak is another sign of H-type Frenkel exciton formation.[68] A final piece of evidence can be obtained by comparing the radiative rates (k_{rad}) of **4a** and **6a**. These two molecules have similar fluorescence lifetimes of 235±10 ps as shown in Figure 4b, but the quantum yield of **4a** (0.06) is half that of **6a** (0.12), so we find k_{rad} = 0.25 ns^{-1} for **4a** and k_{rad} = 0.48 ns^{-1} for **6a**. The decreased k_{rad} value for **4a** is consistent with the low-lying emitting state having a weaker TDM, exactly as expected for an H-type aggregate. All three measurements (absorption lineshape, fluorescence lineshape, and radiative rate) are consistent with the idea that the cage structure supports the formation of neutral H-type excitons.

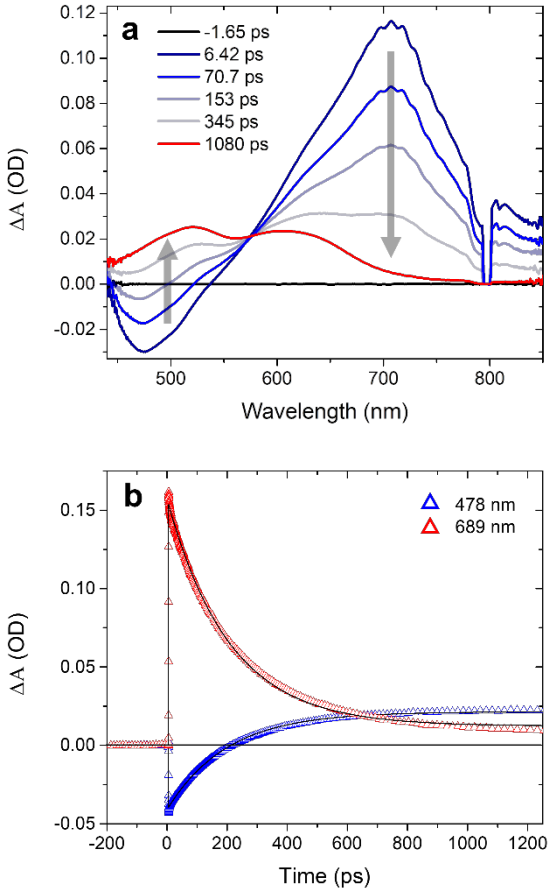

Figure 5. (a) TA spectra over time of phenyl-capped cage **4a** in chloroform. Arrows indicate spectral decline and growth over time. (b) Corresponding kinetic decays at selected wavelengths of initial negative signal (480 nm) and ESA (710 nm).

The last question is whether the modified cage excited state undergoes significantly different dynamics. To investigate the excited state relaxation dynamics, we utilized femtosecond transient absorption (fs-TA) experiments. Figure 5a shows the evolution of the TA spectrum of cage **4a** after 400 nm excitation. An initial excited state absorption (ESA) peaked at ~710 nm, along with a negative signal at 480 nm, appears immediately after excitation. The ESA decays and is replaced by a weaker absorbance with a double peak at 520 and 600 nm that remains constant over the 1.1 ns time range of the experiment, which we assign to the $T_1 \rightarrow T_n$ absorption. Global analysis shows only a single relaxation time of 203 ps required to adequately describe the time-dependent TA dynamics across multiple wavelengths (Figure 5b). The ESA decay is slightly faster than the measured fluorescence decay time, but their similar dynamics suggest that both observables correspond to the initially excited singlet state, which undergoes ISC to the triplet manifold. The fs-TA data for monomer **6a** are very similar to those in Figure 5 (Supporting Information, Figure SI-22), but with a slightly shorter singlet decay time of 190 ps. For both **4a** and **6a**, the rapid ~200 ps ISC time and blue-shifted $T_1 \rightarrow T_n$ ESA are consistent with the fs-TA behavior of other oligothiophene compounds, where ISC is the dominant nonradiative decay pathway.[69-71]

Table 1. Time-resolved photoluminescence (TRPL) and TA lifetimes of compounds 4a and 6a.

	Parameter	4a	6a
TRPL	τ_{PL} (ps)	229	244
TA	τ_{PL} (ps)	203	190
	Φ_{PL}	0.057	0.116
	k_{rad} (ns^{-1})	0.249	0.475

The quantum yields (Φ_{PL}) and radiative rates (k_{rad}) are compared showing **4a**'s decreased radiative rate. Radiative rates are calculated using TRPL photoluminescence lifetimes, $k_{rad} = {}^{\Phi_{PL}}/_{\tau_{PL}}$.

C. Active Triazine Linker and CT States in Compounds 4b and 6b

The substitution of a triazine cap for the phenyl group has only a modest effect on the absorption spectrum of cage **4b** as compared to **4a**. Both cage compounds exhibit similar blue-shifted absorptions dominated by the bithiophene chromophore. Interestingly, the absorption of the corresponding monomer **6b** is broader and even exhibits a weak CT band at around 500 nm. As discussed above, we attribute the broadening to conformational disorder that is partially removed by the cage structure, and the CT feature probably originates from one of these monomer conformations. When compared to **4a**, the main difference is seen in the fluorescence spectrum, which shifts from 450 nm to 550 nm and loses all vibronic structure. **4b**'s fluorescence peak position is also sensitive to solvent polarity, suggesting that the emitting state has CT character (Supporting Information, Figure SI-13). The total fluorescence quantum yield for **4b** is 0.24, significantly greater than that of **4a**. Finally, when the fluorescence decays are examined, **4b** is found to undergo a biexponential decay (Figure 6b). Its emission has a short component similar to those of the monomers (298 ps), but the majority of the fluorescence is emitted with a much longer lifetime of 4.3 ns. The decay time of the long-lived component (4.3 ns) is about 6× greater than that of the analogous triazine-capped monomer **6a** (0.77 ns). The fluorescence spectrum redshifts slightly over the course of the decay (Supporting Information, Figure SI-19), suggesting that the two lifetimes reflect two different CT states. Examining the solvent dependence of the decay, the relative amplitude of the long component increases in more polar solvents, as does its lifetime (Supporting Information, Figure SI-20 and Table SI-18). This is again consistent with the long-lived state having CT character, since more polar solvents tend to favor charge separation and slow down recombination.

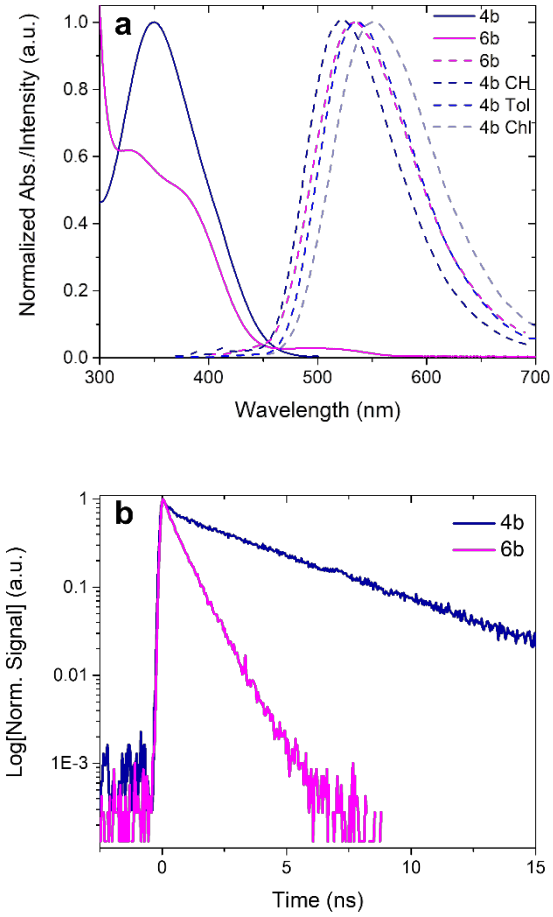

Figure 6. (a) UV-vis spectra (solid) and emission spectra (dashed) of triazine-capped bithiophene cage (**4b**, blue) and triazine-capped monomer (**6b**, pink). The emission of **4b** is shown in three solvents, cyclohexane (CH), toluene (Tol), and chloroform (Chl), to show the red-shifted emission peak as solvent polarity increases. For the emission spectra, a 350 nm excitation wavelength was used. (b) Fluorescence decays of cage **4b** (blue) and monomer **6b** (pink).

There is no sign of a CT absorption feature in Figure 6a, so the emissive CT state must form via relaxation from the neutral absorbing state of **4b**. fs-TA experiments (Figure 7a) are consistent with rapid relaxation into a CT state. First, there is a ~7 ps component that mainly reflects the loss of the stimulated emission feature and growth of an induced absorption around

500 nm, accompanied by a slight shifting of the main ESA feature at 650 nm. This rapid relaxation was not observed in **4a** and can be assigned to the formation of a CT state from the initially excited Frenkel exciton. This initial decay is followed by a 300 ps process that mainly affects the large ESA peak at 650 nm, causing it to lose intensity and shift out to 700 nm. The long-lived ESA has different spectral features from the triplet ESA of **4a**, with a major peak at 700 nm instead of two weaker peaks centered around 500 and 600 nm. Since the 650 nm ESA peak decay is not accompanied by the growth of any other feature, including in the region expected for the $T_1 \rightarrow T_n$ ESA, we think it represents a subpopulation of CT states (possibly due to a different cage conformation) that undergo rapid internal conversion back to the ground state.

The behavior of **4b** can be compared to that of the corresponding monomer **6b** (bithiophene with triazine termination), which undergoes a similar 7 ps relaxation to the CT state, followed by a 350 ps decay that likely reflects rapid internal conversion and possibly some ISC to form a long-lived triplet with ESA features at 500 and 600 nm (Supporting Information, Figures SI-26 and SI-27). However, both the long-lived ESA at 700 nm and the long-lived CT emission are absent in **6b**, suggesting that the cage constraints allow **4b**'s CT state to avoid the rapid non-radiative relaxation processes found in **6b**.

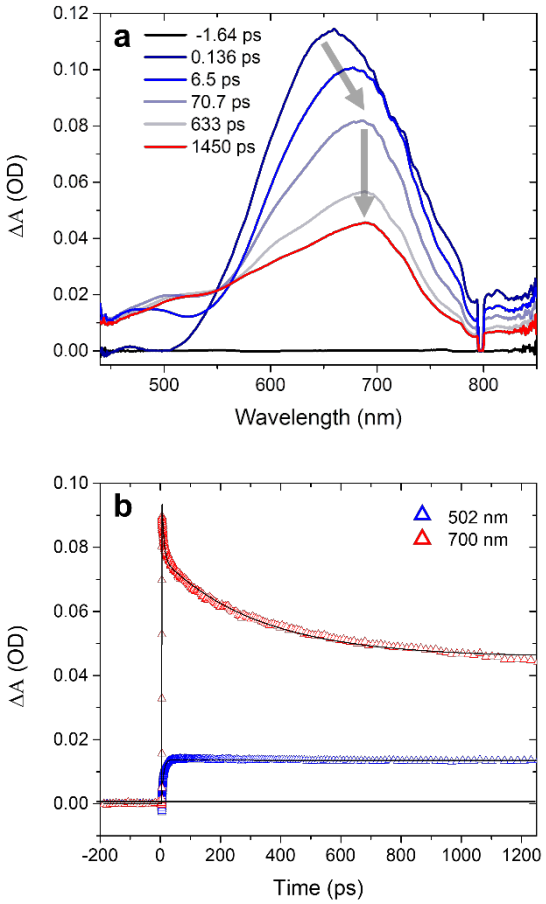

Figure 7. (a) TA spectra over time of triazine-capped cage (**4b**) in chloroform. Arrows indicate shift to longer wavelengths, followed by decay over time. (b) Corresponding kinetic decays at selected wavelengths of induced absorption (500 nm) and long-lived state (700 nm).

Calculations showed that molecular torsions for the monomer **6b** can take place with almost no energetic cost (0.5 kcal/mol or less), confirming its high flexibility. To experimentally mimic the cage constraints, we measured the PL lifetime of 6b in a rigid polymethylmethacrylate polymer matrix. We found a longer lifetime component of 2.4 ns in the polymer (Supporting Information, Figure SI-21), consistent with the idea that increased steric hindrance slows down the nonradiative decay. It is interesting that the solid-state matrix is less effective at preventing this relaxation than the cage in liquid solution.

D. Computational Characterization of the Cage Excited States

The experimental absorption spectra suggest that the cage assembly supports some degree of excitonic character. To clarify how the cage structure modifies the excited electronic states, we turned to time-dependent density functional theory (TDDFT) calculations. Vertical electronic transition calculations for both **4a** and **4b** show that they possess three low-lying

Table 2. TRPL and TA photoluminescent lifetimes of compounds 4b and 6b.

	Parameter	4b	6b
TRPL	τ_1 (ps)	298	277
	τ_2 (ns)	4.30	0.765
TA	τ_1 (ps)	6.64	6.72
	τ_2 (ps)	298	349
	Φ_{PL}	0.238	-
	k_{rad} (ns^{-1})	0.0758	-

Note that the 6 ps decay time in the TA cannot be resolved by the TRPL measurement. The quantum yield (Φ_{PL}) and radiative rate ($\boldsymbol{k_{rad}}$) of **4b** are shown. The radiative lifetime is calculated using the weighted average of the two components from TRPL (0.298 ns (29%) and 4.30 ns (71%)). Therefore, $\tau_{PL} = (0.298 \cdot 0.29) + (4.30 \cdot 0.71) = 3.14\, ns$. Then the radiative rate can be calculated, $k_{rad} = {}^{0.238}/_{3.14} = 0.0758\ \text{ns}^{-1}$.

singlet states corresponding to the interaction of local excitations on the individual branches of the cage (Supporting Information, Figures SI-8 and SI-9), with the highest excited singlet (S_3) in both compounds presenting the largest oscillator strength (Table 3) but with appreciable oscillator strength remaining in the lowest states as well. This trend is consistent with H-type exciton formation, but to confirm this we performed additional calculations with a systematic series of approximations to isolate the effects of conformational disorder versus electronic coupling, concentrating on cage **4a**.

First, we considered three individual capped bithiophene monomers with the frozen cage geometry without any intermolecular coupling. The three computed energies of each bright S_1 state show a sizeable variation due to the different monomer structures within the cage, with each excitation energy close to the S_1-S_3 energies in the complete cage. Although different monomer conformations within the cage help explain the shifts in energy, the oscillator strengths of S_1 for the three monomers are relatively unaffected within this approximation, with values in the 0.91-0.94 and 0.74-0.88 range for monomers in **4b** and

4a, respectively. Second, we turned on electronic interactions between the subunits using several levels of approximation. The center-to-center spatial separation between bithiophene units lies in the range 5.1-5.7 Å, similar to the size of the chromophore itself. The close proximity suggests that the point-dipole approximation will not be adequate, since this tends to overestimate the exciton couplings.[72-74] Indeed, this model overestimated the splitting by ~0.2 eV, as shown in Table 2. The use of a multi-dipole model designed to include molecular size effects can accurately reproduce the cage energies and transition dipole moments from the full quantum calculation. The good agreement suggests that short-range CT interactions triggered by inter-monomer orbital overlap play a minor role (at most) in the main absorption band of cages **4a** and **4b**. To confirm this, we analyzed the three lowest singlet-singlet transitions using a non-bonded trimer model obtained by removing the benzene and triazine (top and bottom) capping rings in **4a** and **4b**, respectively. Calculated excitation energies and oscillator strengths follow the same distribution as in the full cage results, in agreement with a through-space exciton coupling. The main difference is that the energies of the non-bonded trimers are systematically blue-shifted with respect to the cages, which results from the reduction of the effective conjugated length of the system.

Using the multi-dipole model, we can calculate intermolecular exciton coupling constants in the range of 60-80 meV, depending on the chromophore pair. These couplings are larger than those deduced for polythiophene, which range from 5-30 meV depending on the preparation method.[75] The larger coupling may result partly from the short bithiophene segments used in the cage[76], but it is still well below the couplings observed in oligothiophene crystals, which are typically greater than 200 meV.[77-79] The calculations suggest that the cage geometry can achieve electronic couplings intermediate between a disordered polymer and tightly packed crystal, leading to novel excitonic states that have intermediate properties as well.

Table 3. Excitation energies (in eV) and oscillator strengths (in parenthesis) for the three lowest excited singlets computed for non-interacting capped bithiophene (monomers), through the point-dipole and multi-dipole approximation, the non-bonded trimer and the full cage for compounds 4a and 4b.

	ΔE_1 (f_1)	ΔE_2 (f_2)	ΔE_2 (f_2)
Cage 4a			
monomers	3.60 (0.915)	3.61 (0.939)	3.92 (0.911)
point-dipole	3.48 (0.538)	3.57 (0.200)	4.09 (2.191)
multi-dipole	3.54 (0.164)	3.63 (0.970)	3.96 (1.714)
non-bonded trimer	3.63 (0.226)	3.70 (1.046)	3.97 (1.090)
cage	3.52 (0.100)	3.61 (0.840)	3.92 (1.160)
Cage 4b			
monomers	3.64 (0.884)	3.93 (0.743)	4.10 (0.765)
point-dipole	3.55 (0.294)	3.85 (0.172)	4.27 (2.097)
multi-dipole	3.62 (0.492)	3.91 (0.379)	4.14 (1.597)
non-bonded trimer	3.74 (0.672)	4.10 (0.397)	4.21 (1.274)
cage	3.60 (0.440)	3.90 (0.340)	4.12 (1.070)

The calculations show that the initial absorption event creates a neutral excited state in both **4a** and **4b**, consistent with their similar absorption spectra, but after that their paths diverge. Table 3 summarizes the full quantum calculations of the low-lying neutral states of **4b**, and they are similar to those of **4a**. Unlike **4a**, however, electronic structure calculations indicate that **4b** also supports multiple low-lying singlet states with CT character. Excited state optimization of **4b** identifies low energy CT state minima with reduced gaps to the ground state and non-vanishing oscillator strengths (Table 4). All three low-lying states in this geometry (CT_1, CT_2 and CT_3) exhibit significant CT character, in which bithiophene moieties and triazine rings act as electron donor and acceptor groups, respectively (Supporting Information, Figure SI-10). On the other hand, the CT states in cage **4a** are computed at much higher energies, and their involvement in the decay of photo-excited cage **4a** seems energetically forbidden. This result is consistent with the experimental observation of an emissive CT state in **4b** that is reached by picosecond relaxation from the Franck-Condon geometry.

Finally, we note that the calculated oscillator strengths agree qualitatively with the trends observed experimentally. If we compare the neutral ^{1}FE states of **4a** and **6a**, we find that the computed ratio of 1.02:0.71=1.4 is not far from the experimental k_{rad} ratio of 0.48/0.25=1.9. If we compare the neutral exciton state of **4a** with the CT state of **4b**, we find the experimental k_{rad} ratio 0.25/0.08=3.1 is greater than the calculated ratio of oscillator strengths, 0.71:0.43=1.7, but consistent with the observation that the CT state retains significant oscillator strength.

Table 4. Vertical and relative energies (in eV) and oscillator strengths at excited state minima of monomers 6b and 6a, and cages 4b and 4a.

Compound	State	E_{vert}	ΔE	Strength
Monomer 6a	^{1}FE	2.85	-0.68[a]	1.02
Cage 4a	^{1}FE	2.79	-0.45[a] / -1.075[b]	0.71
	^{1}CT	3.43	0.41[a] / 0.005[b]	0.01
Monomer 6b	^{1}CT	2.86	-0.55[a]	0.30
Cage 4b	$^1CT_1$	2.64	-0.22[a] / -0.78[b]	0.43
	$^1CT_2$	2.93	-0.17[a] / -0.73[b]	0.51
	$^1CT_3$	3.14	0.14[a] / -0.41[b]	0.12

FE: Frenkel exciton; CT: charge transfer state. [a]Computed with respect to the vertical excitation energy of S_1 at the ground state geometry. [b]Computed with respect to the vertical excitation energy of S_3 at the ground state geometry.

DISCUSSION

The photophysical behaviors of **4a** and **4b** are summarized in the Jablonski diagrams in Figure 8. Based on the experimental and computational results in the previous sections, we can draw several conclusions. First, the lowest vertical transitions in cages **4a** and **4b** reflect two main contributions: (i) conformational disorder between the three coupled moieties, and (ii) through-space inter-chromophore Coulomb interaction. In fact, the calculations show that the blue shift in the absorbance is primarily the result of the constrained cage shifting the localized excited state and not the formation of a fully delocalized H-type exciton. The S_3 excited states in Figure 8 are more

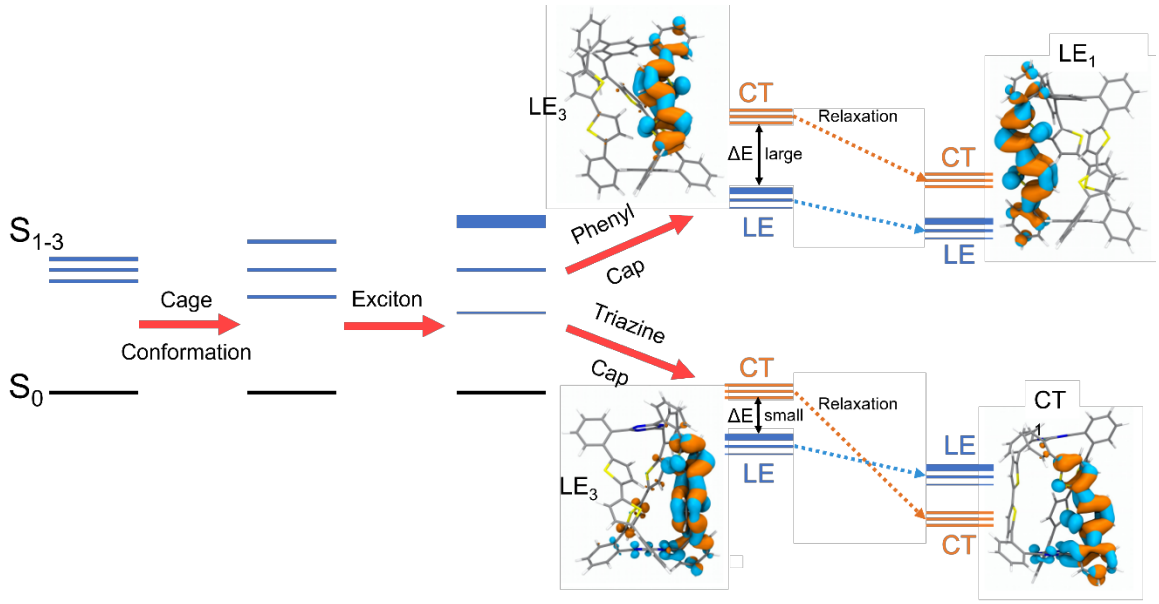

Figure 8. Jablonski diagram representing the singlet energy level shifting from three non-interacting capped bithiophenes to capped bithiophene cages and then the excitonic state. Then the schematic outline of the relaxation processes in the phenyl-capped cage (**4a**) is shown, along with the main (88% of the transition) electron/hole pair densities for the S3 state. The schematic outline of relaxation processes in the trazine-capped cage (**4b**) is shown, along with the main (95% of the transition) showing the electron/hole pair densities (blue/orange) for the lowest CT state.

localized than calculated exciton states in phenyl-cored dendrimers[80], possibly due to the orthogonality of the capping groups. It is remarkable that both theory and experiment show that through-space Coulombic interactions enable the S_3 state to steal considerable oscillator strength from the lower energy states, despite the fact that visually the wavefunctions show limited delocalization. This illustrates how subtle through-space chromophore-chromophore interactions can affect the electronic properties of the cage even with orthogonal phenylene caps that prevent through-bond orbital interactions. Modifying the chromophore "walls" by using moieties with different TDM strengths or orientations could modify the strength of the intermolecular coupling and allow the construction of more delocalized Frenkel exciton states with different properties, e.g. enhanced radiative rates (superradiance).

While the initial excited state is determined by the chromophore wall geometry, its subsequent fate can be controlled by the linker properties. For the inert capping group of **4a**, the ISC rate appears to be largely unaffected by exciton state formation, which acts mainly to reduce the competing radiative rate. For cage **4b**, the initially excited state is similar to that of **4a**, but rapidly relaxes into a CT state, a fraction of which survives for 4.3 ns. The use of the triazine cap introduces a conformationally restricted CT state that can largely avoid the rapid ISC and internal conversion that quench the fluorescence of monomer **6a**, enhancing the fluorescence quantum yield of **4b** relative to **4a**. **4b**'s CT state has significant electron-hole overlap, as can be seen from Figure 8, leading to a singlet-triplet energy gap greater than 1.0 eV (Supporting Information, Table SI-16). This large gap prevents facile intersystem crossing, as observed in thermally activated delayed fluorescence emitters that have a greater degree of charge separation. The ability of thiophene CT states to avoid ISC has been observed in previous work[34], but the origin of this ability has yet to be satisfactorily explained.

The overall picture that emerges is that different elements of the cage structure can be used to control different time periods of the assembly photophysics. The initial excited state structure is largely determined by the geometry of the chromophore walls, and the detailed chemical structure of the caps has little impact on the structure of this state. But the subsequent relaxation of this excitonic state, from picoseconds onward, depends strongly on the nature of the capping group. A non-interacting cap simply allows the chromophore's intrinsic relaxation to proceed (e.g. ISC), but a different cap structure can open up new pathways (e.g. CT) that can outcompete the intrinsic processes. In this way, the cage approach could enable the use of different wall/cap module combinations to rationally design the photophysical behavior of molecular chromophore assemblies.

CONCLUSIONS

The newly developed cage-type architecture enables the construction of multi-chromophoric molecules with tunable linkers. Although the cage framework still has some flexibility even with its additional bonding constraints, it provides the opportunity to examine assemblies of bithiophene chromophores in two limits: inert linkers that support through-space interchromophore interactions, and active linkers that modify the electronic states. The first type of linker is demonstrated by the phenyl cap which enables H-type Frenkel exciton formation. This excitonic state still undergoes facile ISC but the weak TDM of the low-lying emitting state suppresses the fluorescence output by a factor of 2. The use of a triazine cap, on the other hand, introduces low-lying CT states that can avoid ISC and enhance the fluorescence yield. Both capping groups lead to low-lying neutral excitonic states with weaker oscillator strengths, but the triazine linker provides a new CT relaxation

pathway that can avoid ISC and generate a higher overall fluorescence quantum yield. While many workers have shown how covalently linking chromophores can produce new excited states, this paper shows how chemical tuning can precisely control the nature of those states, even for the same geometrical arrangement. These results provide a new route toward structurally well-defined multichromophoric assemblies whose excited states can be rationally designed using the tools of organic synthesis and computational chemistry.

ASSOCIATED CONTENT

Supporting Information. Experimental procedures and spectroscopic data for all new compounds (^{1}H NMR, ^{13}C NMR, IR, HRMS), including images of NMR spectra and HPLC traces for racemic and enantiomerically enriched compounds. Single crystal X-ray diffraction data for compounds **4a** and **4b**. Computational details are provided, including monomer and cage lowest energy conformations, excited state NTOs, and charge transfer relaxation. Additional spectroscopic data, including steady-state measurements, quantum yield calculations, time-resolved photoluminescence fits, and additional transient absorption spectra, are included.

AUTHOR INFORMATION

Author Contributions.
T. N. L., C.T. and W. G. S. contributed equally to this work.

Corresponding Authors
*mkrische@mail.utexas.edu
*david.casanova@ehu.eus
*christob@ucr.edu

ORCID
Taylor N. Lewis: 0000-0001-6096-4432
Claire Tonnelé: 0000-0003-0791-8239
Michael J. Krische: 0000-0001-8418-9709
David Casanova: 0000-0002-8893-7089
Christopher J. Bardeen: 0000-0002-5755-9476

Notes
The authors declare no competing financial interest.

ACKNOWLEDGMENT

C. J. B. acknowledges support from the National Science Foundation grant CHE-1800187. D. C. and C. T. thank the Ministerio de Economía y Competitividad of Spain (projects PID2019-109555GB-I00 and RED2018-102815-T) and the Eusko Jaurlaritza (project PIBA19-0004) and are thankful for the technical and human support provided by DIPC Computer Center. M. J. K. acknowledges the Robert A. Welch Foundation (F-0038) and the National Science Foundation (CHE-1855744) for partial support of this research.

REFERENCES

1. Pope, M.; Swenberg, C. E., *Electronic Processes in Organic Crystals and Polymers*. 2 ed.; Oxford Science: New York, NY, 1999.
2. Gust, D.; Moore, T. A.; Moore, A. L., Mimicking Photosynthetic Solar Energy Transduction. *J. Am. Chem. Soc.* **2001,** *34*, 40–48.
3. Amanpour, J.; Hu, G.; Alexy, E. J.; Mandal, A. K.; Kang, H. S.; Yuen, J. M.; Diers, J. R.; Bocian, D. F.; Lindsey, J. S.; Holten, D., Tuning the Electronic Structure and Properties of Perylene–Porphyrin–Perylene Panchromatic Absorbers. *J. Phys. Chem. A* **2016,** *120*, 7434–7450.
4. Whited, M. T.; Niral M. Patel; Roberts, S. T.; Allen, K.; Djurovich, P. I.; Bradforth, S. E.; Thompson, M. E., Symmetry-breaking intramolecular charge transfer in the excited state of meso-linked BODIPY dyads. *Chem. Commun.* **2012,** *48*, 284-286.
5. Bartynski, A. N.; Gruber, M.; Das, S.; Rangan, S.; Mollinger, S.; Trinh, C.; Bradforth, S. E.; Vandewal, K.; Salleo, A.; Bartynski, R. A.; Bruetting, W.; Thompson, M. E., Symmetry-Breaking Charge Transfer in a Zinc Chlorodipyrrin Acceptor for High Open Circuit Voltage Organic Photovoltaics. *J. Am. Chem. Soc.* **2015,** *137*, 5397–5405.
6. Métivier, R.; Kulzer, F.; Weil, T.; Müllen, K.; Basché, T., Energy Transfer Rates and Pathways of Single Donor Chromophores in a Multichromophoric Dendrimer Built around a Central Acceptor Core. *J. Am. Chem. Soc.* **2004,** *126*, 14364–14365.
7. Liu, D.; Feyter, S. D.; Cotlet, M.; Stefan, A.; Wiesler, U.-M.; Herrmann, A.; Grebel-Koehler, D.; Qu, J.; Müllen, K.; Schryver, F. C. D., Fluorescence and Intramolecular Energy Transfer in Polyphenylene Dendrimers. *Macromolecules* **2003,** *36*, 5918–5925.
8. Hsiao, J.-S.; Krueger, B. P.; Wagner, R. W.; Johnson, T. E.; Delaney, J. K.; Mauzerall, D. C.; Fleming, G. R.; Lindsey, J. S.; Bocian, D. F.; Donohoe, R. J., Soluble Synthetic Multiporphyrin Arrays. 2. Photodynamics of Energy-Transfer Processes. *J. Am. Chem. Soc.* **1996,** *118*, 11181–11193.
9. Hindin, E.; Forties, R. A.; Loewe, R. S.; Ambroise, A.; Kirmaier, C.; Bocian, D. F.; Lindsey, J. S.; Holten, D.; Knox, R. S., Excited-State Energy Flow in Covalently Linked Multiporphyrin Arrays: The Essential Contribution of Energy Transfer between Nonadjacent Chromophores. *J. Phys. Chem. B* **2004,** *108*, 12821–12832.
10. Thomas, K. R. J.; Thompson, A. L.; Sivakumar, A. V.; Bardeen, C. J.; Thayumanavan, S., Energy and Electron Transfer in Bifunctional Non-Conjugated Dendrimers. *J. Am. Chem. Soc.* **2005,** *127*, 373-383.
11. Melinger, J. S.; Pan, Y.; Kleiman, V. D.; Peng, Z.; Davis, B. L.; McMorrow, D.; Lu, M., Optical and Photophysical Properties of Light-Harvesting Phenylacetylene Monodendrons Based on Unsymmetrical Branching. *J. Am. Chem. Soc.* **2002,** *124*, 12002–12012.
12. Ghiggino, K. P.; Reek, J. N. H.; Crossley, M. J.; Bosman, A. W.; Schenning, A. P. H. J.; Meijer, E. W., The Dynamics of Electronic Energy Transfer in Novel Multiporphyrin Functionalized Dendrimers: A Time-Resolved Fluorescence Anisotropy Study. *J. Phys. Chem. B* **2000,** *104*, 2596–2606.
13. Jiang, D.-L.; Aida, T., Photoisomerization in dendrimers by harvesting of low-energy photons. *Nature* **1997,** *388*, 454–456.
14. Muller, A. M.; Avlasevich, Y. S.; Schoeller, W. W.; Mullen, K.; Bardeen, C. J., Exciton Fission and Fusion in Bis(tetracene) Molecules with Different Covalent Linker Structures. *J. Am. Chem. Soc.* **2007,** *129*, 14240-14250.
15. Korovina, N. V.; Joy, J.; Feng, X.; Feltenberger, C.; Krylov, A. I.; Bradforth, S. E.; Thompson, M. E., Linker-Dependent Singlet Fission in Tetracene Dimers. *J. Am. Chem. Soc.* **2018,** *140*, 10179−10190.
16. Sanders, S. N.; Kumarasamy, E.; Pun, A. B.; Trinh, M. T.; Choi, B.; Xia, J.; Taffet, E. J.; Low, J. Z.; Miller, J. R.; Roy, X.; X.-Y. Zhu; Steigerwald, M. L.; Sfeir, M. Y.; Campos, L. M., Quantitative Intramolecular Singlet Fission in Bipentacenes. *J. Am. Chem. Soc.* **2015,** *137*, 8965−8972.
17. Pun, A. B.; Asadpoordarvish, A.; Kumarasamy, E.; Tayebjee, M. J. Y.; Niesner, D.; McCamey, D. R.; Sanders, S. N.; Campos, L. M.; Sfeir, M. Y., Ultra-fast intramolecular singlet fission to persistent multiexcitons by molecular design. *Nat. Chem.* **2019,** *11*, 821–828.
18. Johnson, J. C.; Akdag, A.; Zamadar, M.; Chen, X.; Schwerin, A. F.; Paci, I.; Smith, M. B.; Havlas, Z. k.; Miller, J. R.; Ratner, M. A.; Nozik, A. J.; Michl, J., Toward Designed Singlet Fission: Solution Photophysics of Two Indirectly Coupled Covalent Dimers of 1,3-Diphenylisobenzofuran. *J. Phys. Chem. B* **2013,** *117*, 4680−4695.
19. Akdag, A.; Wahab, A.; Beran, P.; Rulíšek, L.; Dron, P. I.; Ludvík, J. í.; Michl, a. J., Covalent Dimers of 1,3-Diphenylisobenzofuran for Singlet Fission: Synthesis and Electrochemistry. *J. Org. Chem.* **2015,** *80*, 80−89.

20. Basel, B. S.; Zirzlmeier, J.; Hetzer, C.; Phelan, B. T.; Krzyaniak, M. D.; Reddy, S. R.; Coto, P. B.; Horwitz, N. E.; Young, R. M.; White, F. J.; Hampel, F.; Clark, T.; Thoss, M.; Tykwinski, R. R.; Wasielewski, M. R.; Guldi, D. M., Unified model for singlet fission within a non-conjugated covalent pentacene dimer. *Nat. Commun.* **2016,** *8*, 15171.

21. Margulies, E. A.; Miller, C. E.; Wu, Y.; Ma, L.; Schatz, G. C.; Young, R. M.; Wasielewski, M. R., Enabling singlet fission by controlling intramolecular charge transfer in π-stacked covalent terrylenediimide dimers. *Nat. Chem.* **2016,** *8*, 1120-1125.

22. Serin, J. M.; Brousmiche, D. W.; Fréchet, J. M. J., Cascade energy transfer in a conformationally mobile multichromophoric dendrimer. *Chem. Commun.* **2002**, 2605-2607.

23. Ahn, T.-S.; Nantalaksakul, A.; Dasari, R. R.; Al-Kaysi, R. O.; Müller, A. M.; Thayumanavan, S.; Bardeen, C. J., Energy and Charge Transfer Dynamics in Fully Decorated Benzyl Ether Dendrimers and Their Disubstituted Analogues. *J. Phys. Chem. B* **2006,** *110*, 24331–24339.

24. Zhang, Y.; Wang, Z.; Ng, M.-K.; Rothberg, L. J., Conformational Reorganization and Solvation Dynamics of Dendritic Oligothiophenes. *J. Phys. Chem. B* **2007,** *111*, 13211–13216.

25. Harvey, P. D.; Brégier, F.; Aly, S. M.; Szmytkowski, J.; Paige, M. F.; Steer, R. P., Dendron to Central Core S_1–S_1 and S_2–S_n (n>1) Energy Transfers in Artificial Special Pairs Containing Dendrimers with Limited Numbers of Conformations. *Chem. Eur. J.* **2013,** *19*, 4352-4368.

26. Ondarse-Alvarez, D.; Kömürlü, S.; Roitberg, A. E.; Pierdominici-Sottile, G.; Tretiak, S.; Fernandez-Alberti, S.; Kleiman, V. D., Ultrafast electronic energy relaxation in a conjugated dendrimer leading to inter-branch energy redistribution. *Phys. Chem. Chem. Phys.* **2016,** *18*, 25080-25089.

27. Pasman, P.; Rob, F.; Verhoeven, J. W., Intramolecular charge-transfer absorption and emission resulting from through-bond interaction in bichromophoric molecules. *J. Am. Chem. Soc.* **1982,** *104*, 5127–5133.

28. Heitele, H.; Michel-Beyerle, M. E., Electron transfer through aromatic spacers in bridged electron-donor-acceptor molecules. *J. Am. Chem. Soc.* **1985,** *107*, 8286–8288.

29. Paddon-Row, M. N., Investigating long-range electron-transfer processes with rigid, covalently linked donor-(norbornylogous bridge)-acceptor systems. *Acc. Chem. Res.* **1994,** *27*, 18–25.

30. Clayton, A. H. A.; Scholes, G. D.; Ghiggino, K. P.; Paddon-Row, M. N., Through-Bond and Through-Space Coupling in Photoinduced Electron and Energy Transfer: An ab Initio and Semiempirical Study. *J. Phys. Chem.* **1996,** *100*, 10912–10918.

31. Davis, W. B.; Svec, W. A.; Ratner, M. A.; Wasielewski, M. R., Molecular-wire behaviour in p -phenylenevinylene oligomers. *Nature* **1998,** *396*, 60-63.

32. Kilså, K.; Kajanus, J.; Macpherson, A. N.; Mårtensson, J.; Albinsson, B., Bridge-Dependent Electron Transfer in Porphyrin-Based Donor−Bridge−Acceptor Systems. *J. Am. Chem. Soc.* **2001,** *123*, 3069–3080.

33. Thompson, A. L.; Ahn, T.-S.; Thomas, K. R. J.; Thayumanavan, S.; Martínez, T. J.; Bardeen, C. J., Using Meta Conjugation To Enhance Charge Separation versus Charge Recombination in Phenylacetylene Donor−Bridge−Acceptor Complexes. *J. Am. Chem. Soc.* **2005,** *127*, 16348–16349.

34. Cruz, C. D.; Christensen, P. R.; Chronister, E. L.; Casanova, D.; Wolf, M. O.; Bardeen, C. J., Sulfur-Bridged Terthiophene Dimers: How Sulfur Oxidation State Controls Interchromophore Electronic Coupling. *J. Am. Chem. Soc.* **2015,** *137*, 12552–12564.

35. Cruz, C. D.; Yuan, J.; Climent, C.; Tierce, N. T.; Christensen, P. R.; Chronister, E. L.; Casanova, D.; Wolf, M. O.; Bardeen, C. J., Using sulfur bridge oxidation to control electronic coupling and photochemistry in covalent anthracene dimers. *Chem. Sci.* **2019,** *10*, 7561–7573.

36. Kumarasamy, E.; Sanders, S. N.; Tayebjee, M. J. Y.; Asadpoordarvish, A.; Hele, T. J. H.; Fuemmeler, E. G.; Pun, A. B.; Yablon, L. M.; Low, J. Z.; Paley, D. W.; Dean, J. C.; Choi, B.; Scholes, G. D.; Steigerwald, M. L.; Ananth, N.; McCamey, D. R.; Sfeir, M. Y.; Campos, L. M., Tuning Singlet Fission in π-Bridge-π Chromophores. *J. Am. Chem. Soc.* **2017,** *139*, 12488−12494.

37. Geary, L. M.; Glasspoole, B. W.; Kim, M. M.; Krische, M. J., Successive C−C Coupling of Dienes to Vicinally Dioxygenated Hydrocarbons: Ruthenium Catalyzed [4 + 2] Cycloaddition across the Diol, Hydroxycarbonyl, or Dione Oxidation Levels. *J. Am. Chem. Soc.* **2013,** *135*, 3796−3799.

38. Geary, L. M.; Chen, T.-Y.; Montgomery, T. P.; Krische, M. J., Benzannulation via Ruthenium-Catalyzed Diol−Diene [4+2] Cycloaddition: One- and Two-Directional Syntheses of Fluoranthenes and Acenes. *J. Am. Chem. Soc.* **2014,** *136*, 5920−5922.

39. Kasun, Z. A.; Sato, H.; Nie, J.; Mori, Y.; Bender, J. A.; Roberts, S. T.; Krische, M. J., Alternating oligo(o,p-phenylenes) via ruthenium catalyzed diol–diene benzannulation: orthogonality to cross-coupling enables de novo nanographene and PAH construction. *Chem. Sci.* **2018,** *9*, 7866–7873.

40. Suravarapu, S. R.; Parvathaneni, S. P.; Bender, J. A.; Roberts, S. T.; Krische, M. J., Benzannulation through Ruthenium(0)-Catalyzed Transfer Hydrogenative Cycloaddition: Precision Synthesis and Photophysical Characterization of Soluble Diindenoperylenes. *Chem. Eur. J.* **2020,** *26*, 7504–7510.

41. Shuler, W. G.; Parvathaneni, S. P.; Rodriguez, J. B.; Lewis, T. N.; Berges, A. J.; Bardeen, C. J.; Krische, M. J., Synthesis and Photophysical Properties of Soluble N-Doped Rubicenes via Ruthenium-Catalyzed Transfer Hydrogenative Benzannulation. *Chem. Eur. J.* **2021,** *27*, 4898–4902.

42. Sato, H.; Bender, J. A.; Roberts, S. T.; Krische, M. J., Helical Rod-like Phenylene Cages via Ruthenium Catalyzed Diol-Diene Benzannulation: A Cord of Three Strands. *J. Am. Chem. Soc.* **2018,** *140*, 2455−2459.

43. Sato, H.; Blemker, M. A.; Hellinghausen, G.; Armstrong, D. W.; Nafie, J. W.; Roberts, S. T.; Krische, M. J., Triple Helical Ir(ppy)3 Phenylene Cage Prepared by Diol-Mediated Benzannulation: Synthesis, Resolution, Absolute Stereochemistry and Photophysical Properties. *Chem. Eur. J.* **2019,** *25*, 8719–8724.

44. Rupert, B. L.; Mitchell, W. J.; Ferguson, A. J.; Kose, M. E.; Rance, W. L.; Rumbles, G.; Ginley, D. S.; Shaheen, S. E.; Kopidakis, N., Low-bandgap thiophene dendrimers for improved light harvesting. *J. Mater. Chem.* **2009,** *19*, 5311–5324.

45. Zhang, J.; Fischer, M. K. R.; Bäuerle, P.; Theodore Goodson, Energy Migration in Dendritic Oligothiophene-Perylene Bisimides. *J. Phys. Chem. B* **2013,** *117*, 4204−4215.

46. Petrella, A.; Cremer, J.; Cola, L. D.; Bauerle, P.; Williams, R. M., Charge Transfer Processes in Conjugated Triarylamine-Oligothiophene-Perylenemonoimide Dendrimers. *J. Phys. Chem. A* **2005,** *109*, 11687-11695.

47. Tsuge, A.; Hara, T.; Moriguchi, T.; Yamaji, M., Preparation, Structure, and Spectral Properties of Cyclophanes Consisting of Oligothiophene Units. *Chem. Lett.* **2008,** *37*, 870-871.

48. Fischer, M. K. R.; Kaiser, T. E.; Wurthner, F.; Bauerle, P., Dendritic oligothiophene-perylene bisimide hybrids: synthesis, optical and electrochemical properties. *J. Mater. Chem.* **2009,** *19*, 1129–1141.

49. Mishra, A.; Ma, C.-Q.; Janssen, R. A. J.; Bauerle, P., Shape-Persistent Oligothienylene–Ethynylene-Based Dendrimers: Synthesis, Spectroscopy and Electrochemical Characterization. *Chem. Eur. J.* **2009,** *15*, 13521–13534.

50. Rance, W. L.; Rupert, B. L.; Mitchell, W. J.; Kose, M. E.; Ginley, D. S.; Shaheen, S. E.; Rumbles, G.; Kopidakis, N., Conjugated Thiophene Dendrimer with an Electron-Withdrawing Core and Electron-Rich Dendrons: How the Molecular Structure Affects the Morphology and Performance of Dendrimer:Fullerene Photovoltaic Devices. *J. Phys. Chem. C* **2010,** *114*, 22269–22276.

51. Pandolfi, F.; Rocco, D.; Mattiello, L., Synthesis and characterization of new D–π-A and A–π-D–π-A type oligothiophene derivatives. *Org. Biomol. Chem.* **2019,** *17*, 3018-3025.

52. Wu, J.; Baumgarten, M.; Debije, M. G.; Warman, J. M.; Mullen, K., Arylamine-Substituted Hexa-perihexabenzocoronenes: Facile Synthesis and Their Potential Applications as “Coaxial” Hole-Transport Materials. *Angew. Chem.* **2004,** *116*, 5445–5449.

53. Lipshutz, B. H.; Wilhelm, R. S.; Floyd, D. M., Chemistry of higher order, mixed organocuprates. 1. Substitution reactions at unactivated secondary centers. *J. Am. Chem. Soc.* **1981,** *103*, 7672–7674.
54. Kabira, S. M. H.; Iyodaa, M., Selectivity of Cyano-Gilman Cuprates: Synthesis of 10-Membered Ring Cyclophanes. *Chem. Commun.* **2000**, 2329–2330.
55. Miyake, Y.; Wu, M.; Rahmana, M. J.; Iyoda, M., Novel Electron-Transfer Oxidation of Lipshutz Cuprates with 1,4-Benzoquinones: An Efficient Homo-Coupling Reaction of Aryl Halides and Its Application to The Construction of Macrocyclic Systems. *Chem. Commun.* **2005**, 411-413.
56. Iyoda, M.; Rahman, M. J.; Matsumoto, A.; Wu, M.; Kuwatani, Y.; Nakao, K.; Miyake, Y., Synthesis of Nonaphenylenes and Dodecaphenylenes Using Electron-transfer Oxidation of Lipshutz Cuprate Intermediates. *Chem. Lett.* **2005,** *34*, 1474-1475.
57. Miyake, Y.; Wu, M.; Rahman, M. J.; Kuwatani, Y.; Iyoda, M., Efficient Construction of Biaryls and Macrocyclic Cyclophanes via Electron-Transfer Oxidation of Lipshutz Cuprates. *J. Org. Chem.* **2006,** *71*, 6110–6117.
58. Rahman, M. J.; Yamakawa, J.; Matsumoto, A.; Enozawa, H.; Nishinaga, T.; Kamada, K.; Iyoda, M., Synthesis of Nonaphenylenes and Dodecaphenylenes Using Electron-Transfer Oxidation of Lipshutz Cuprates and Formation of Nanostructural Materials from Hexadodecyloxynonaphenylene. *J. Org. Chem.* **2008,** *73*, 5542–5548.
59. Lukevics, E.; Arsenyan, P.; Belyakov, S.; Popelis, J.; Pudova, O., Cycloaddition Reactions of Nitrile Oxides to 2,4-Silyl- and Germyl-Substituted Thiophene-1,1-dioxides. *Organometallics* **2001,** *20*, 2487–2491.
60. Nielsen, C. B.; Angerhofer, A.; Abboud, K. A.; Reynolds, J. R., Discrete Photopatternable π-Conjugated Oligomers for Electrochromic Devices. *J. Am. Chem. Soc.* **2008,** *130*, 9734–9746.
61. Chao, C. S.; Cheng, C. H.; Chang, C. T., New method for the preparation of activated nickel and cobalt powders and their application in biaryl synthesis. *J. Org. Chem.* **1983,** *48*, 4904-4907.
62. Zhou, Z.-h.; Yamamoto, T., Research on carbon—carbon coupling reactions of haloaromatic compounds mediated by zerovalent nickel complexes. Preparation of cyclic oligomers of thiophene and benzene and stable anthrylnickel(II) complexes. *J. Organomet. Chem.* **1991,** *414*, 119-127.
63. Segawa, Y.; Miyamoto, S.; Omachi, H.; Matsuura, S.; Šenel, P.; Sasamori, T.; Tokitoh, N.; Itami, K., Concise Synthesis and Crystal Structure of [12]Cycloparaphenylene. *Angew. Chem. Intl. Ed.* **2011,** *50*.
64. Segawa, Y.; Šenel, P.; Matsuura, S.; Omachi, H.; Itami, K., [9]Cycloparaphenylene: Nickel-mediated Synthesis and Crystal Structure. *Chem. Lett.* **2011,** *40*, 423-425.
65. Janietz, D.; Bauer, M., A New Facile Synthesis of 2-Substituted 4,6-Diphenyl-1,3,5-triazines. *Synthesis* **1993**, 33-34.
66. Xiao, J.; Liu, X.-K.; Wang, X.-X.; Zheng, C.-J.; Li, F., Tailoring electronic structure of organic host for high-performance phosphorescent organic light-emitting diodes. *Org. Elec.* **2014,** *15*, 2763–2768.
67. Kasha, M.; Rawls, H. R.; El-Bayoumi, M. A., The Exciton Model in Molecular Spectroscopy. *Pure Appl. Chem.* **1965,** *11*, 371-392.
68. Spano, F. C., The Spectral Signatures of Frenkel Polarons in H- and J-Aggregates. *Acc. Chem. Res.* **2010,** *43*, 429-439.
69. Rossi, R.; Ciofalo, M.; Carpita, A.; Ponterini, G., Singlet—triplet intersystem crossing in 2,2′:5′,2″-terthiophene and some of its derivatives. *J. Photochem. Photobiol. A* **1993,** *70*, 59-67.
70. Beljonne, D.; Cornil, J.; Friend, R. H.; Janssen, R. A. J.; Brédas, J. L., Influence of Chain Length and Derivatization on the Lowest Singlet and Triplet States and Intersystem Crossing in Oligothiophenes. *J. Am. Chem. Soc.* **1996,** *118*, 6453–6461.
71. Becker, R. S.; Melo, J. S. d.; Maçanita, A. L.; Elisei, F., Comprehensive Evaluation of the Absorption, Photophysical, Energy Transfer, Structural, and Theoretical Properties of α-Oligothiophenes with One to Seven Rings. *J. Phys. Chem.* **1996,** *100*, 18683–18695.
72. Scholes, G. D., Long-Range Resonance Energy Transfer in Molecular Systems. *Ann. Rev. Phys. Chem.* **2003,** *54*, 57-87.
73. Wong, K. F.; Bagchi, B.; Rossky, P. J., Distance and Orientation Dependence of Excitation Transfer Rates in Conjugated Systems: Beyond the Förster Theory. *J. Phys. Chem. A* **2004,** *108*, 5752-5763.
74. Beljonne, D.; Curutchet, C.; Scholes, G. D.; Silbey, R. J., Beyond Förster Resonance Energy Transfer in Biological and Nanoscale Systems. *J. Phys. Chem. B* **2009,** *113*, 6583-6599.
75. Clark, J.; Silva, C.; Friend, R. H.; Spano, F. C., Role of Intermolecular Coupling in the Photophysics of Disordered Organic Semiconductors: Aggregate Emission in Regioregular Polythiophene. *Phys. Rev. Lett.* **2007,** *98*, 206406.
76. Manas, E. S.; Spano, F. C., Absorption and spontaneous emission in aggregates of conjugated polymers. *J. Chem. Phys.* **1998,** *109*, 8087-8101.
77. Muccini, M.; Schneider, M.; Taliani, C.; Sokolowski, M.; Umbach, E.; Beljonne, D.; Cornil, J.; Bredas, J. L., Effect of wavefunction delocalization on the exciton splitting in organic conjugated materials. *Phys. Rev. B* **2000,** *62*, 6296-6300.
78. Sun, H.; Zhao, Z.; Spano, F. C.; Beljonne, D.; Cornil, J.; Shuai, Z.; BrØdas, J.-L., Absorption and Emission in Quaterthienyl ThinFilms. *Adv. Mater.* **2003,** *15*, 818-822.
79. Tavazzia, S.; Campione, M.; Laicini, M.; Raimondo, L.; Borghesi, A., Measured Davydov splitting in oligothiophene crystals. *J. Chem. Phys.* **2006,** *124*, 194710.
80. Kose, M. E.; Mitchell, W. J.; Kopidakis, N.; Chang, C. H.; Shaheen, S. E.; Kim, K.; Rumbles, G., Theoretical Studies on Conjugated Phenyl-Cored Thiophene Dendrimers for Photovoltaic Applications. *J. Am. Chem. Soc.* **2007,** *129*, 14257-14270.

TOC GRAPHIC